J Mater Sci (2008) 43:4996–5004
DOI 10.1007/s10853-008-2739-2

Effect of cation stoichiometry on the transport properties of calcium ruthenium oxide ceramics

Sezhian Annamalai · Igor Vidensky · Ian L. Pegg · Biprodas Dutta

Received: 7 January 2008 / Accepted: 16 May 2008 / Published online: 3 June 2008

Abstract Seebeck coefficient and electrical resistivity have been determined on a series of compounds having the general composition $Ca_nRu_{1-n}O_y$. From property and structural considerations, these compounds have been divided into two categories: one group resembling Ca_2RuO_4 and the second category exhibiting properties similar to $CaRuO_3$. While the former is an antiferromagnetic insulator, the latter is a paramagnetic metal. The Seebeck coefficient remains relatively unchanged within the members of the two groups, irrespective of the molar ratios of the cations. Even between the two groups of compounds, the Seebeck coefficient exhibits minimal difference even as the cation ratio (Ru/Ca) of the compounds is varied from 0.35 ($n = 0.74$) to 1.94 ($n = 0.34$). The resistivity, however, varies by nine orders of magnitude as the cation ratio is varied in the same range. Consequently, the resulting power factor ($s^2\sigma$, where s is the Seebeck coefficient and σ is the electrical conductivity), which is a measure of the usefulness or thermopower conversion efficiency of a thermoelectric material, is found to vary by nine orders of magnitude.

Introduction

Ceramic oxides containing transition metal ions exhibit a rich spectrum of physical properties including a broad range of technologically important phenomena such as ferromagnetism, ferroelectricity, and superconductivity. One fascinating type is the Ruddlesdon-Popper series with a general chemical formula $A_{n+1}M_nO_{3n+1}$, with 'M' being transition metals such as Ti, Mn, and Ru, and 'A' representing the alkaline earth (Gr. II) elements with 'n' being an integer. Among them, the 4*d*-electron ruthenates (compounds containing ruthenium oxide as one of the components) offer considerable prospects by virtue of exhibiting strong interplay of structural, magnetic, and electronic degrees of freedom. The ruthenates typically have layered crystal structures with a general formula: $A_{n+1}Ru_nO_{3n+1}$, where A is Ca_xSr_{1-x}. Here n may be varied from 1 to ∞; and x may assume any value between 0 and 1 [1]. In terms of their electronic properties, they exhibit strong electron–electron correlation and a number of physical properties such as metal–insulator transition, antiferromagnetism (Ca_2RuO_4) [1, 2], ferromagnetism ($SrRuO_3$ and $Sr_4Ru_3O_{10}$) [3, 4], superconductivity (Sr_2RuO_4) [5], metamagnetism, and magnetoresistivity ($Ca_3Ru_2O_7$) [6]. The structures of these layered materials are such that they allow manipulation of their physical properties by imaginative alteration of composition and by the application of external magnetic fields. In this investigation, Seebeck coefficient and electrical resistivity have been determined on a series of compounds having the general composition $Ca_nRu_{1-n}O_y$. From property and structural considerations, these compounds have been divided into two categories: one group resembling Ca_2RuO_4 and the second category exhibiting properties similar to $CaRuO_3$, which are entirely different from the former. While the former is an antiferromagnetic insulator, the latter is a paramagnetic metal. In the following, a short summary of the electrical and magnetic properties of some important oxides, similar in structure to $CaRuO_3$ and Ca_2RuO_4, is provided.

Among the layered ruthenates, the physical properties of Ca_2RuO_4 and $CaRuO_3$ have been investigated earlier [7–9].

S. Annamalai · I. Vidensky · I. L. Pegg · B. Dutta (✉)
Vitreous State Laboratory, The Catholic University of America, Washington, DC, USA
e-mail: biprodasd@vsl.cua.edu

Ca_2RuO_4 is structurally analogous to the unusual superconductor Sr_2RuO_4, but has very different properties [7–10]. $Ca_2RuO_{4+\delta}$ is a Mott-insulator, which undergoes a first order metal to insulator transition at a temperature between 105 and 300 K, depending on the oxygen content and is antiferromagnetic with a Néel temperature of around 110 K [11]. Its properties are very sensitive to chemical composition [12–14] and even hydrostatic pressure [15]. For example, application of hydrostatic pressure or substitution of Ca^{2+} by La^{3+} or Sr^{2+} can convert the antiferromagnetic insulating state to a metallic state, and even induce weak ferromagnetism. The family of orthorhombic perovskite compounds $CaMO_3$ (M = Ru and Fe) have evoked considerable interest on account of their unusual magnetic properties [16–19]. The magnetic ground state of $CaRuO_3$ (Ru^{4+}, $4d^4$: $t_{2g}{}^4e_g{}^0$ with $S = 1$) is controversial. Recent publications indicate paramagnetic behavior (or exchange enhanced paramagnetism) down to 30 mK [16–19]. On the other hand, high and low temperature resistivity results indicate that $CaRuO_3$ is a non-Fermi liquid metal [17].

It is well established that the isostructural $SrRuO_3$ is a ferromagnet (FM) with a Curie temperature $T_C = 165$ K. The stark contrast of the magnetic properties of $SrRuO_3$ and $CaRuO_3$ is surprising because the closed shell s-like character of Sr and Ca does not contribute to the density of states at the Fermi surface and therefore should not be the origin for the different magnetic ground states of these two compounds. Since a common structural feature of the two compounds is that they are composed of an array of corner-shared RuO_6 octahedra, it is assumed that the degree of tilting and rotation of these octahedra within their ideal cubic-perovskite structure governs the observed differences in the magnetic and also the transport properties.

In $CaRuO_3$, a narrow itinerant 4*d* band is formed through hybridization of Ru-t_{2g} and O-2*p* orbitals. The 4*d* bandwidth thus formed sensitively depends on degree of hybridization [20], which also determines the mobility of carriers, leading to electric conduction. $CaRuO_3$ is believed to have a narrow itinerant 4*d* bandwidth (narrower than for $SrRuO_3$), which is too narrow for long range magnetic ordering, but not so narrow as to cause $CaRuO_3$ to be non-metallic [21]. It means that calcium ruthenate is on the verge of magnetic ordering which also should demonstrate a metal–insulator transition with even a slight variation in the cation ratio (Ru/Ca) of the composition $CaRuO_3$.

Ruthenium addition has shown to drastically reduce the resistivity without a large increase in thermal conductivity in the technologically important Ca-manganites, which also exhibit large thermopower [22, 23]. Hence, understanding the transport mechanism in ceramics containing ruthenium oxides is of prime importance. The ruthenates also have a misfit layered structure, typical of most of the important thermoelectric ceramic oxides such as sodium and calcium cobaltites [22]. In this study, we have investigated the Seebeck coefficient and electrical resistivity of a series of calcium ruthenium oxides having the general composition $Ca_nRu_{1-n}O_y$. The transport properties of such oxides were studied as the cation ratio (Ru/Ca) was systematically varied. X-ray diffraction (XRD) analyses, supported by electron microscopic investigation, have been employed to understand the variation of the properties with composition. The thermopower and resistivity data have been discussed in the light of the general properties exhibited by Ca_2RuO_4 and $CaRuO_3$, and possible implications of such data on the use of calcium ruthenates as prospective thermoelectric materials have also been considered.

Experimental procedure

Seven samples from the series of general composition $Ca_nRu_{1-n}O_y$, were prepared with '*n*' varying between 0.34 and 0.74 (Table 1). The stoichiometry of oxygen, viz., the value of '*y*' was allowed to reach its natural level by sintering the ceramic in ambient atmosphere and was not experimentally determined. Sample batches were prepared by mixing the stoichiometric amounts of reagent grade oxides, viz., CaO (in the form of $CaCO_3$) and RuO_2 in three stages for optimal mixing of the ingredients. The oxide

Table 1 Composition and thermoelectric properties of $Ca_nRu_{1-n}O_y$

Sample ID	Molar composition		Resistivity at 380 K $\rho(\Omega m)$	Seebeck coefficient at 380 K s($\mu V\ K^{-1}$)	Power factor (s^2/ρ) ($Wm^{-1}\ K^{-2}$)	Ru/Ca ratio
	CaO	RuO_2				
CaR-1	0.74	0.26	2.00E+04	26	3.38E−14	0.35
CaR-2	0.72	0.28	2.00E+00	29	4.21E−10	0.39
CaR-3	0.67	0.33	1.20E−01	28	6.53E−09	0.49
CaR-4	0.57	0.43	1.00E−03	36	1.30E−06	0.75
CaR-5	0.54	0.46	8.00E−05	35	1.53E−05	0.85
CaR-6	0.42	0.58	4.00E−05	38	3.61E−05	1.38
CaR-7	0.34	0.66	3.00E−05	32	3.41E−05	1.94

powders were first weighed in a Metler balance to an accuracy of three decimal places (1 mg) and ground/mixed in an alumina mortar and pestle. The mixed powder was then transferred to an alumina crucible and calcined in a box furnace at 873 K for 4 h. The heating rate to the final temperature was maintained at 200 K/h. After soaking the powder mix for 4 h at 873 K, it was cooled to room temperature by switching off the furnace. The crucible was removed from the furnace and the contents were again mixed in a mortar and pestle. Thereafter, the mixture was calcined a second time after transferring it back to the same alumina crucible at 1,073 K for 4 h. At the end of the second calcination procedure, the contents from the crucible were removed and mixed in a mortar and pestle for a third time. Multiple calcinations allowed intimate mixing of the oxide powders and also removed all the CO_2 gas that may have been generated during the calcinations of $CaCO_3$. Following the mixing of the calcined powders for a third time, the powder was dry-pressed to form pellets (1 cm diameter, 0.5 cm thick) in a hydraulic press, capable of applying up to 25,000 psi ($\sim$172 MPa) in a cylindrical die. Typically, 5,000 psi ($\sim$34 MPa) was employed during the preparation of samples in this investigation. The dry-pressed pellets were placed on fresh alumina/fireclay substrates and were finally sintered at 1,173 K for 10 h in air inside a box furnace. At the end of the sintering procedure, the samples were furnace-cooled at a rate of 100 K/h to room temperature. The procedure described was optimized to produce reproducible samples as determined from X-ray diffraction and X-ray fluoroscopy measurements of ground specimens.

Several identical pellets of each composition were prepared using the procedure outlined above. One such pellet would be crushed into powder for X-ray fluorescence spectroscopy (XRF) analysis for confirmation of sample composition as listed in Table 1. The same powder would then be used for X-ray diffraction analysis (Thermo ARL-X'tra Difractometer) using Cu–K_α radiation. Analysis of the XRD patterns was performed by refining the diffraction data by a commercial software (Jade), in the pattern-matching mode to identify the phase compositions of the samples. The microstructures of polished surfaces of the samples were analyzed by scanning electron microscopy couples with energy dispersive spectroscopy (SEM/EDS) (Jeol, JXA-35A). Such analyses were used to verify if multiple phases were present in the samples.

Electrical resistivity was measured using the Van der Pauw four-probe method [24]. A fully computerized apparatus, capable of scanning between 82 and 700 K (H-50 and K-20, MMR Technologies, Mountain View, CA), was used to determine resistivity of materials. Resistivity measurements were conducted in a dark chamber, maintained at 8–10 mTorr vacuum under ohmic conditions. Silver leads were attached to four points on the top surface of the pellets with silver paste which served as the electrodes. The samples were coplanar with a maximum thickness of about 2 mm. Two electrodes would be used to pass a pre-determined current (10^{-12}–10^{-2} A) through the sample, while the other two electrodes would be used to measure the voltage generated. The current and voltage measurements would then be combined by a conformal mapping procedure to compute the resistivity of the sample [24]. At any temperature, the current and voltage measurements were performed by using different sets of current and voltage probes. For example, the current probes in one measurement would be used as voltage probes in the next. Before a measurement, the sample would be maintained at a particular temperature for a pre-determined time (15 min for each mm of sample thickness) to achieve temperature equilibration. In all, 24 resistivity measurements were performed at each temperature and the average of these values comprise the resistivity data presented in Table 1. The error in temperature measurement was determined at 0.5 K and that of the conductivity measurements is estimated at $\pm$7%.

Thermopower (Seebeck coefficient) of the samples was measured using a computerized apparatus (SB-100 and K-20, MMR Technologies, Mountain View, CA). A schematic of the experimental setup is provided in Fig. 1. The sample and a NIST traceable standard (constantan wire) were pasted across the heat sink and sources as shown in the figure. The resistance heater was activated by passing a desired current through it. The heat flux generated by the heater would create a temperature difference between the heat source and heat sink which would be the same for the sample as well as the standard (i.e., between 'b' and 'c' in Fig. 1). The temperature difference across the sample was allowed to stabilize and achieve steady-state by allowing a 300 s soaking period. After the expiry of the soaking period, the voltage generated across the length of the sample was measured. The geometry of the sample would typically be 4 mm in length and $\sim$1 mm in width, embedded on copper heat-sink and heat-source. Sixteen measurements of thermopower were made at each temperature and the average of such measurements reported. The temperature differential (usually maintained between 1 and 2 K) generates thermo-voltage across the sample as well as the

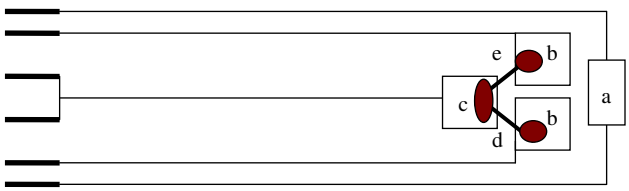

Fig. 1 Schematic of Seebeck coefficient measurement system. a—Resistance heater, b—heat source, c—heat sink, d—reference constantan wire, e—sample

standard constantan wire which are measured by a suitable voltmeter in the SB-100 system. Given the thermopower (μV/K) of the standard constantan wire, the temperature difference (ΔT) giving rise to its measured thermo-voltage (V_c) was determined by the controlling software of the measurement system. While the thermo-voltage generated by the sample (V_s) was also measured by the SB-100, the Seebeck coefficient or thermopower ($V_s/\Delta T$) was readily calculated by the software. The error in temperature determination was estimated at 0.1 K and that of thermopower measurement is determined at ±10%.

Results and discussion

Compositions of the seven samples prepared for this investigation are listed in Table 1. The estimated error in the determination of composition by XRF analysis is ±5%. The molar compositions and the ratios of the cations (Ru/Ca or the molar ratios of ruthenium to calcium ions) of all the samples have been provided in Table 1. The resistivity (ρ) and thermopower (s) measured at 380 K of all the samples are also listed in Table 1 and Figs. 2 and 3. The values of thermopower factor ($s^2\sigma$, where s is the Seebeck coefficient and σ is the electrical conductivity) of the samples, calculated from the experimentally determined

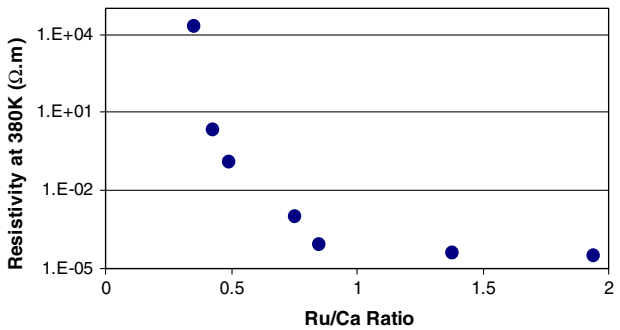

Fig. 2 Electrical resistivity of $Ca_nRu_{1-n}O_y$ samples as a function of Ru/Ca ratio

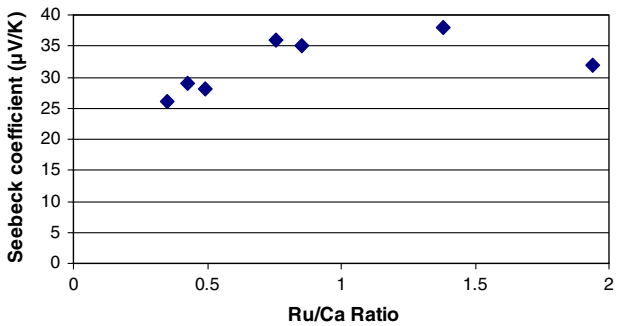

Fig. 3 Thermopower of $Ca_nRu_{1-n}O_y$ samples as a function of Ru/Ca ratio

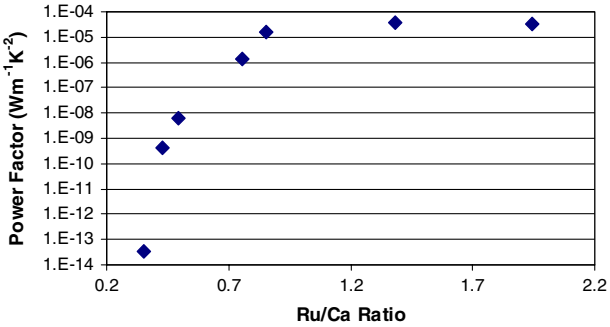

Fig. 4 Power factor ($S^2\sigma$) values for $Ca_nRu_{1-n}O_y$ samples as a function of Ru/Ca ratio

Seebeck coefficient and electrical conductivity ($1/\rho$), are listed in Table 1 and also depicted in Fig. 4.

The effect of Ru substitution on resistivity of the $Ca_nRu_{1-n}O_y$ system as n is varied between 0.74 and 0.34 is quite dramatic as observed in Table 1 and Fig 2. As Ru concentration is increased from 26 mol% (CaR-1, $n = 0.74$, Ru/Ca = 0.35), the resistivity decreases sharply, initially. The resistivity is observed to decrease by three orders of magnitude as Ru is increased to 30 mol% (CaR-2, Ru/Ca = 0.39). When the Ru concentration is further increased to 33 mol% (CaR-3, Ru/Ca = 0.49) the resistivity decreases further by more than an order of magnitude: i.e., from 2 to 0.12 Ωm. The resistivity continues to drop as Ru concentration is increased further, though at a decreasing rate, until 46 mol% Ru is reached. Any further increase in Ru concentration does not lead to significant reduction in resistivity.

The compounds CaR-1–CaR-4 have relatively large resistivity values (2×10^4–1×10^{-3} Ωm) and their X-ray diffraction patterns (Fig. 5) are strikingly similar to that of the well-known antiferromagnetic Mott insulator Ca_2RuO_4 (same as the composition CaR-3). Moreover, as observed in Table 1 and Fig. 2, dc conductivity is very sensitive to composition. As demonstrated by previous workers [12–14], and confirmed by the resistivity data of CaR-3, the resistivity varies by orders of magnitude with modest changes in Ru/Ca ratio. The second group of compositions, viz., CaR-5–CaR-7 has characteristic low resistivities (8×10^{-5}–3×10^{-5} Ωm) and the X-ray diffraction patterns are similar to that of $CaRuO_3$ (Fig. 6). The resistivities vary in the small range 3×10^{-5}–8×10^{-5} Ωm and appear almost invariant in the log ρ scale of Fig. 2.

The variation in resistivity with Ru/Ca ratio is also reflected in the activation energy for the electrical conduction (Table 1 and Figs. 7, 8). The activation energies for dc transport have been determined from Arrhenius plots of ln σ versus $1/T$ which are provided in Fig 7. The first group of samples (viz., Ca_2RuO_4 group) has higher activation energies which decrease with increasing Ru/Ca ratio. It is observed that the activation energy of

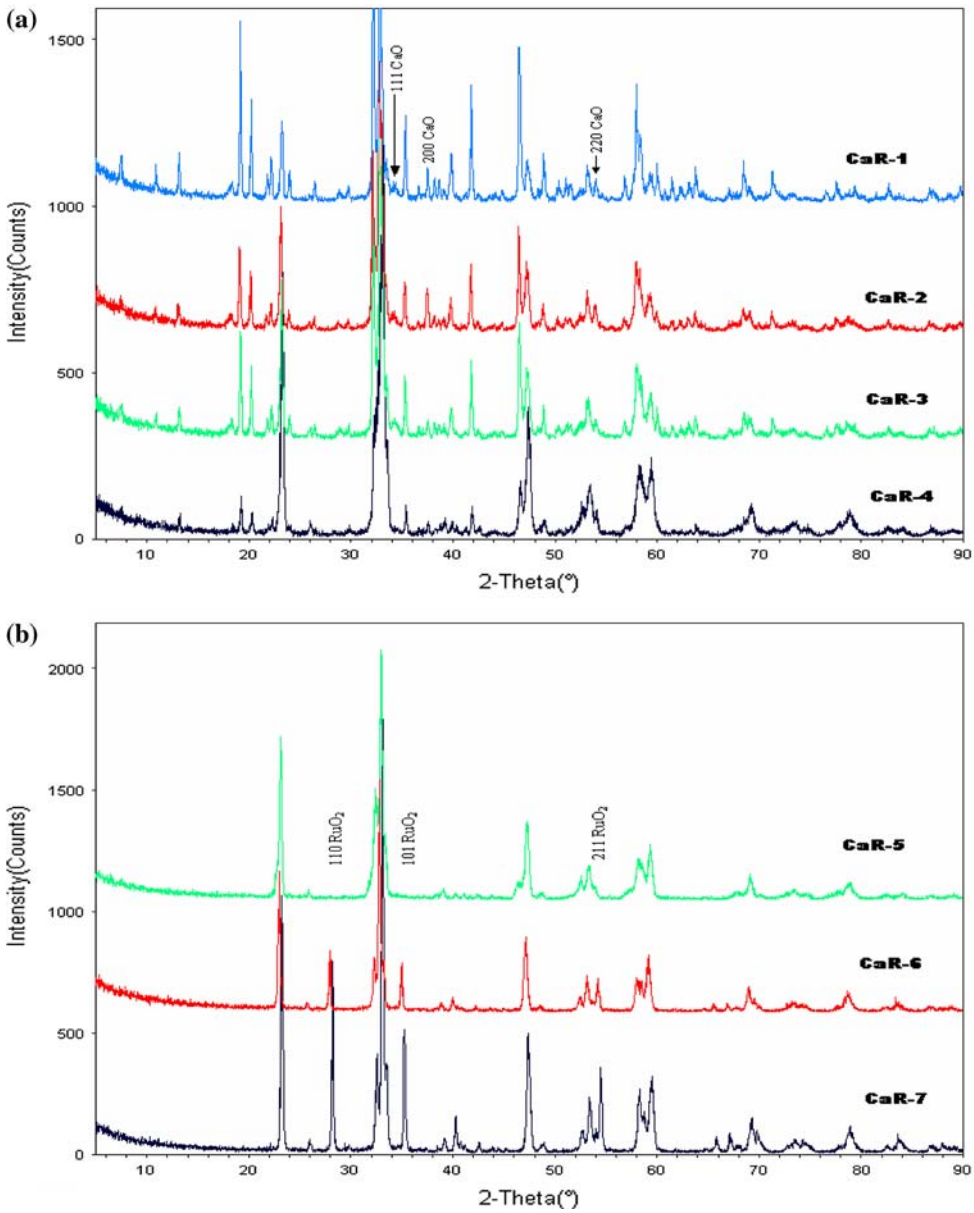

Fig. 5 (**a**) XRD patterns of CaR-1, -2, -3, and -4 showing Ca_2RuO_4 and CaO (minor) phases. (**b**) XRD patterns of CaR-5, -6, and -7 showing $CaRuO_3$ and RuO_2 (monor) phases

CaR-1–CaR-4 (Ca_2RuO_4 group) is very sensitive to Ru/Ca ratio and the dramatic variation in resistivity appears accounted for by variation in activation energy. We also observe that each of these (CaR-1–CaR-4) compositions (Ca_2RuO_4 group) exhibits small polaronic behavior, shown by the change in the slope of their ln σ (σ being the electrical conductivity) versus temperature curve. The higher temperature (380–500 K) activation energies are almost twice that of their lower temperature (300–380 K) values. The second group of compositions, viz., CaR-5–CaR-7 ($CaRuO_3$ group) has lower activation energy approaching zero and is found insensitive to the cation ratio. This behavior is indicative of metallic transport.

Mott and Davis [25] suggest that the occurrence of small polaronic transport in a semiconductor may be discerned by the difference in activation energy determined from its thermopower and resistivity measurements. In the case of transport due to band transport of "bare" electrons or holes, the activation energies determined from both techniques are identical. However, in the case of small polarons, they would be significantly different. The activation energy in small polaronic systems has been found to be significantly lower than that determined from resistivity data. Bosman and Crevecoeur [26] plotted log ρ versus $1/T$ as well as 2.3(k/e)s versus $1/T$ (where ρ is the resistivity, s is the Seebeck coefficient, k is the Boltzmann's constant, e the electronic charge, and T is the absolute temperature) for Li-doped NiO polycrystalline materials. The identical slopes observed in their data is indicative of activation energies being very similar in thermopower and dc transport. Such results provide

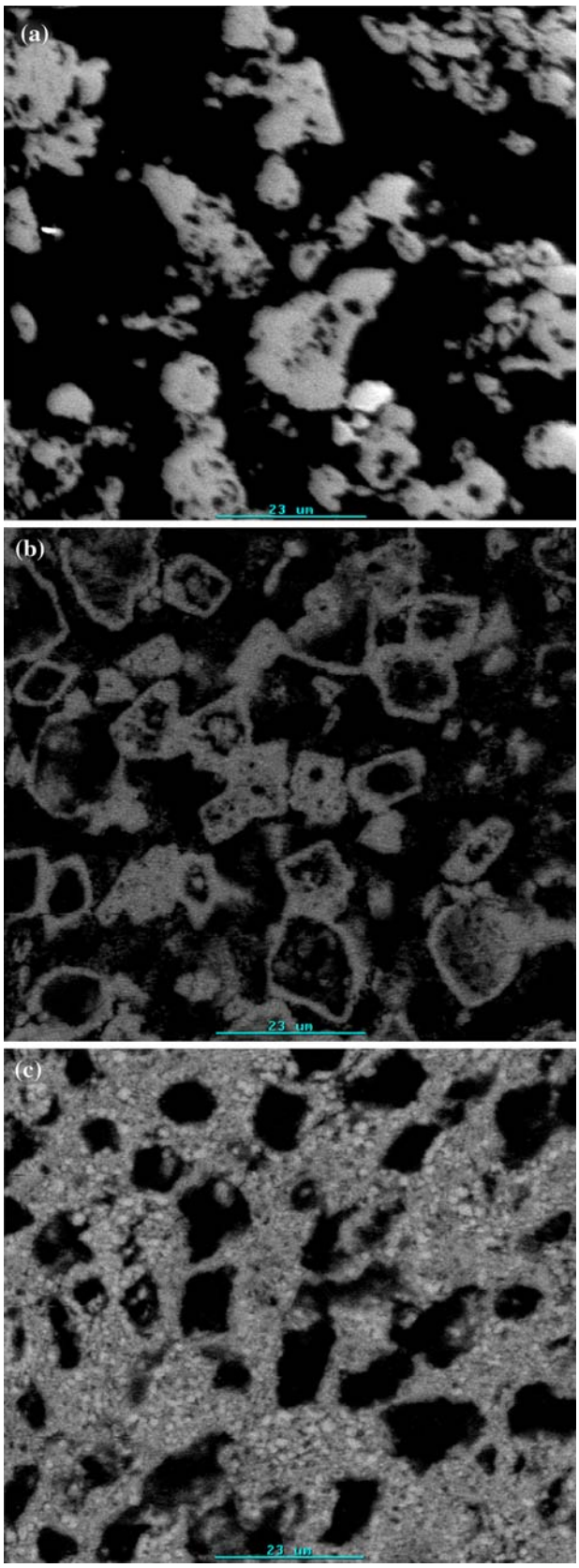

Fig. 6 (**a**) SEM image of CaR-6 (×1000, 23 μm). (**b**) Microstructure of CaR-5. (**c**) Microstructure of CaR-2

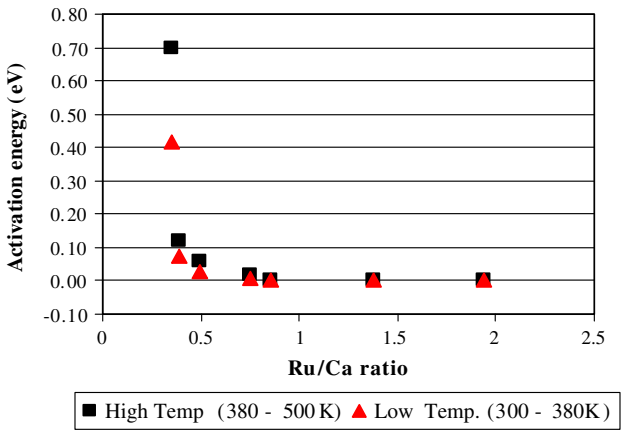

Fig. 7 Activation energy for conduction of $Ca_nRu_{1-n}O_y$ samples as a function of Ru/Ca ratio

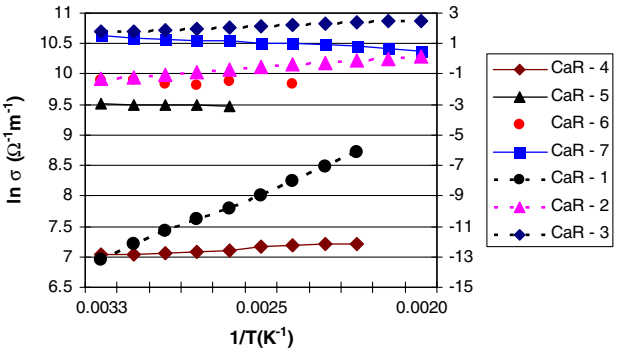

Fig. 8 Conductivity of $Ca_nRu_{1-n}O_y$ samples as a function of inverse temperature (CaR-1–CaR-3 on the secondary *y*-axis)

conclusive proof that small polarons do not participate in the transport process of such materials [25]. A similar analysis performed for the Ca_2RuO_4 group (CaR-1–CaR-4) reveals that the ratio of activation energies (conduction/thermopower) varies from 16 to 312 for different samples, strongly indicating small polaronic behavior. The same ratio for the $CaRuO_3$ group varies from 0.69 to 4.5, which indicates a more metallic behavior.

The Seebeck coefficient, measured at 380 K, for all the samples are provided in Table 1 and depicted in Fig. 3 as a function of composition. The effect of cation stoichiometry on Seebeck coefficient is absolutely different from that observed for resistivity. As Ru concentration is increased from 26 (CaR-1) to 66 mol% (CaR-7), the Seebeck coefficient varies in the small range of +26 to +38 μV/K. While, the resistivity decreases by nine orders of magnitude, the Seebeck coefficient increases just marginally. This feature is quite novel because thermopower increases with resistivity, especially in insulators and semiconductors. However, as depicted in Fig. 3, even for such a small variation in thermopower, the compositions represented by CaR-1, -2, -3, -4 (Ca_2RuO_4 group of oxides) and those

represented by $CaRuO_3$ (CaR-5, -6, -7) can be grouped separately. In other words, the members of the Ca_2RuO_4 group have Seebeck coefficient varying from +26 to +36 μV/K, while the members of the $CaRuO_3$ group have Seebeck coefficient varying from +32 to +38 μV/K.

The power factor (Table 1 and Fig. 4) varies by nine orders of magnitude, from 3.38×10^{-14} to 3.41×10^{-5} Wm^{-1} K^{-2}, for the composition range studied. Again, as expected from the variation trend of resistivity and thermopower, $s^2\sigma$ initially increases sharply, from3.38×10^{-14} to 1.3×10^{-6} Wm^{-1} K^{-2} (CaR-1–CaR-4), after which the power factor does not change much for the CaR-5–CaR-7 compounds. Again, as observed for the resistivity and Seebeck coefficient data, the oxides can be divided into two groups, viz., the Ca_2RuO_4 and $CaRuO_3$ group of compounds. While, the Ca_2RuO_4 group has lower power factor, as expected from low conductivity and s values, the $CaRuO_3$ group has substantially higher power factors. The fact that the thermopower of CaR-7 is 10^9 times larger than that of CaR-1 implies that the thermopower conversion efficiency is dramatically enhanced. Such a large variation is technologically important where the interest is to discover the novel thermoelectric materials having large thermopower conversion efficiencies. In the present case, the dramatic increase in power factor has been made possible by a cation ratio (Ru/Ca) variation of 0.35 (CaR-1)–1.94 (CaR-7) in the $Ca_nRu_{1-n}O_y$ system.

Thermoelectric materials are used to convert heat into electrical energy directly via the Seebeck effect, and conversely, a current may be flown through the material to remove heat by virtue of the Peltier effect. The performance of a thermoelectric material is given by the dimensionless figure of merit $ZT = s^2T(\sigma/\kappa)$, where s is the thermopower, T is the absolute temperature, σ is the electrical conductivity, and κ is the thermal conductivity. For achieving optimum thermoelectric efficiency, a material should have large thermopower (Seebeck coefficient), low electrical resistivity, and low thermal conductivity. In most materials, these three properties are dependent on one another. For example, in metals, an increase in electrical conductivity normally leads to a concomitant increase in thermal conductivity and decrease in thermopower, which does not allow large improvements in ZT value. On the other hand, electrical insulators may have large thermopower but are highly resistive, rendering them ineffective as thermoelectric materials. For that reason, increasing the thermopower factor in the same system by varying the cation ratio is considered extremely significant. However, it is important to note that such an increase in $s^2\sigma$ will have to be coupled with lower thermal conductivity values for achieving a decent ZT value. The next target of the present investigation is to determine thermal conductivity as a function of Ru/Ca ratio in these oxides.

In any ceramic system, it is important to link the properties investigated to the phases present. The problem becomes complicated if multiple phases appear when a cation is substituted by another. In such circumstances it is not straightforward to determine which of the phases are responsible for any property change that may be observed. In the present investigation, SEM/EDS analyses performed on the samples reveal that substitution of Ru for Ca or vice versa in the range of compositions presented in Table 1 does not lead to the formation of a significant second phase as shown in Fig. 6a–c. In Fig. 6c, the black regions are actually the pores and not any major second phase as determined by EDS analyses [unpublished work]. This feature is also supported by the X-ray diffraction patterns of the samples depicted in Fig. 5 where only one phase is detected. CaR-5 is closest in composition to $CaRuO_3$ and the only phase observed in it resembles the diffraction pattern of $CaRuO_3$ as determined by the commercially available search-match routine of the "JADE" program. Samples CaR-6 and CaR-7, which have Ru/Ca ratio of greater than one, have higher RuO_2 than CaR-5. As expected, a second phase (with the composition of RuO_2) is observed along with the $CaRuO_3$ phase in samples CaR-6 and CaR-7. While sample CaR-3 has the exact composition of Ca_2RuO_4 with a Ru/Ca ratio of 0.5, CaR-1, and CaR-2 have greater CaO concentrations. Sample CaR-4, however, has a somewhat lower concentration of CaO as compared to the Ca_2RuO_4 composition. All the samples represented by CaR-1 through CaR-4 have very similar XRD characteristic spectra, except for variation in the intensity of different peaks. From the SEM/EDS and XRD data, it seems appropriate to segregate CaR-5 through CaR-7 and CaR-1 through CaR-4 in two distinct structural groups which bear resemblance to $CaRuO_3$ and Ca_2RuO_4, respectively. A similar segregation of the samples was justified on the basis of resistivity data in a previous section.

While $CaRuO_3$ is a paramagnetic metal, the compound Ca_2RuO_4 is an antiferromagnetic insulator and both have a perovskite-type structure [22]. Accordingly, the resistivity of the compound closest in composition to $CaRuO_3$ (CaR-5; $\rho = 8 \times 10^{-5}$ Ωm) is about four orders of magnitude less than that of CaR-3 ($\rho = 1.2 \times 10^{-1}$ Ωm), which is closest in composition to Ca_2RuO_4. Interestingly both groups of compounds (viz., those found similar to $CaRuO_3$ and Ca_2RuO_4) have very close Seebeck coefficients: +35 and +28 μV/K, respectively, despite the fact that they have such large differences in resistivity. Clearly, the transport phenomenon contributing to thermopower is different from that contributing to electrical conduction.

Similar behavior was observed in $SrRuO_3$ by Klein et al. [27] who studied the influence of the doping level by Seebeck coefficient measurements. Such measurements are

particularly suitable for studying the transport properties of polycrystalline ceramics because this technique is not sensitive to grain boundary effects. Klein et al. found that the Seebeck coefficient was found to be only slightly affected by a variety of cation substitutions or by temperature (in the temperature range of 293–400 K), a feature observed in the present investigation in the $Ca_nRu_{1-n}O_y$ system too. The value of Seebeck coefficient for $SrRuO_3$ was reported to be +34 μV/K at room temperature, confirming the whole character of the carriers. In the present work, the thermopower of the sample resembling $CaRuO_3$ in cation stoichiometry (CaR-5) is +35 μV/K, signifying that the electronic structure and especially the density of states of these ceramics (e.g., $SrRuO_3$ and $CaRuO_3$) are unaffected not only by the various substitutions but also by the type of the cation apart from Ru.

A comprehensive model predicting the Seebeck coefficient in ruthenate ceramics does not exist. However, we shall use Heikes formula [27] to understand the thermopower behavior of the $Ca_nRu_{1-n}O_y$ system. The Heikes formula is given by:

$$S = -[k/e]\ln\{[(2S_n + 1)/(2S_{n+1} + 1)][(1 - x/x)]\}$$

where k is the Boltzmann's constant, e the electronic charge, x is the carrier concentration, and S_n and S_{n+1} correspond to the spins of the transition metal M^{n+} and $M^{(n+1)+}$, respectively. The near-invariance of the thermopower data (Table 1 and Figs. 3, 4), regardless of the Ru/Ca ratio, indicates that the charge doping term $-[k/e]\ln[(1 - x)/x]$ of the Heikes formula has almost no influence on the thermopower, conclusively proving that the generalized Heikes formula does not apply here.

The electrical conductivity, however, has been observed to be extremely sensitive to the Ru/Ca stoichiometry as depicted in Figs. 2, 7, and 8. A metal–insulator transition is observed at a Ru/Ca ratio of 0.7–0.8, which can be substantiated by a dramatic increase in activation energy at these cation ratios. While the precise origin of such a dramatic transition in resistivity is beyond the scope of this article, it is possible to adopt the models of Cox et al. [20] and Cao et al. [21] and explain the dc resistivity data as follows: the 4*d* band of carriers is formed through hybridization of Ru-t_{2g} and O-2*p* orbitals, the width of which is dependant on the degree of hybridization. The more effective the hybridization is, the higher will be the mobility of carriers. Larger mobility decreases activation energy, and as depicted in Fig. 2, the resistivity decreases exponentially. $CaRuO_3$ is believed to have a narrow itinerant 4*d* bandwidth (narrower than for $SrRuO_3$), which is too narrow for long range magnetic ordering, but not so narrow as to cause $CaRuO_3$ to be non-metallic [21]. Following Cao et al. [21], a metal–insulator transition is expected in $CaRuO_3$ with even a slight variation in the cation ratio (Ru/Ca). This is precisely what has been presented in Figs. 2, 7, and 8 where a slight decrease in the Ru/Ca ratio from CaR-3 increases the resistivity dramatically.

Conclusion

Thermopower and resistivity measurements were conducted on $Ca_nRu_{1-n}O_y$ as n was varied between 0.74 and 0.34. Effective substitution of Ca by Ru ions, without the formation of a substantial second phase, has been demonstrated. Resistivity decreases monotonically as the Ru/Ca ratio is increased. A variation of about nine orders of magnitude in resistivity has been observed over the composition range studied. The thermopower increases marginally with increase in Ru/Ca ratio. However, above a Ru/Ca ratio of 0.75, it remains insensitive to cation ratio. As expected, the thermopower factor of the end members of $Ca_nRu_{1-n}O_y$ varies by nine orders of magnitude. Based on the transport properties, the members of the $Ca_nRu_{1-n}O_y$ series have been grouped as Ca_2RuO_4-type, a Mott-insulator (CaR-1–CaR-4), and $CaRuO_3$-type, a paramagnetic metal (CaR-5–CaR-7). It has been demonstrated the Heikes formula for thermopower is not valid for calcium ruthenates, and the transport mechanism has been explained in terms of the effectiveness of the hybridization of the Ru-t_{2g} and O-2*p* orbitals.

Acknowledgements We gratefully acknowledge the contributions of Niveen Fahmy and Wei Zhao in sample preparation.

References

1. Cao G, McCall S, Shepard M, Crow JE, Guertin RP (1997) Phys Rev B 56:R2916. doi:10.1103/PhysRevB.56.R2916
2. Nakatsuji S, Ikeda SI, Maeno Y (1997) J Phys Soc Jpn 66:1868. doi:10.1143/JPSJ.66.1868
3. Callaghan A, Moller W, Ward R (1966) Inorg Chem 5:1572. doi:10.1021/ic50043a023
4. Crawford MK, Harlow RL et al (2002) Phys Rev B 65:214412. doi:10.1103/PhysRevB.65.214412
5. Maeno Y, Hashimoto H et al (1994) Nature 372:532. doi:10.1038/372532a0
6. Cao G, McCall S et al (1997) Phys Rev Lett 78:1751. doi:10.1103/PhysRevLett.78.1751
7. Eom CB, Cava RJ et al (1992) Science 258:1766. doi:10.1126/science.258.5089.1766
8. Wang X, Xin Y et al (2004) App Phys Lett 85(25):6146
9. Rane S, Prudenziati M, Morten B (2005). J Active Passive Elec Dev 1:123
10. Zurbuchen MA, Jia YF et al (2001) Appl Phys Lett 78:2351. doi:10.1063/1.1364659
11. Braden M, Andre G, Nakatsuji S, Maeno Y (1998) Phys Rev B 58:847. doi:10.1103/PhysRevB.58.847
12. Cao G, McCall S et al (2000) Phys Rev B 61:R5053. doi:10.1103/PhysRevB.61.R5053
13. Fukazawa H, Maeno Y (2001) J Phys Soc Jpn 70:460. doi:10.1143/JPSJ.70.460

14. Nakatsuji S, Maeno Y (2000) Phys Rev Lett 84:2666. doi: 10.1103/PhysRevLett.84.2666
15. Nakamura F, Goko T et al (2002) Phys Rev B 65:220402. doi: 10.1103/PhysRevB.65.220402
16. Gibb TC, Greatrex RG et al (1973) J Chem Soc, Dalton Trans 1253. doi:10.1039/dt9730001253
17. Klein L, Antognazza L et al (1999) Phys Rev B 60:1448. doi: 10.1103/PhysRevB.60.1448
18. Felner I, Nowik I, Bradaric IM, Gospodinov M (2000). Phys Rev B 62:11332. doi:10.1103/PhysRevB.62.11332
19. Friedt O, Braden M et al (2001) Phys Rev B. 63:174432
20. Cox PA, Egdell RG et al (1983) J Phys C Solid State Phys 16:6221. doi:10.1088/0022-3719/16/32/014
21. Cao G, McCall S, Shepard M, Crow JE, Guertin RP (1997) Phys Rev B 56:321. doi:10.1103/PhysRevB.56.321
22. Raveau B, Maignan A (2003) Europhys News 34(6)
23. Hebert S, Martin C et al (2001) Proceedings of the 6th European workshop on thermoelectrics, Freiburg
24. Van der Pauw LJ (1958) Philips Res Rep 13:1
25. Mott NF, Davis EA (1979) Electronic processes in non-crystalline materials. Clarendon Press, London
26. Bossman AL, Crevecoeur C (1966) Phys Rev 144:763. doi: 10.1103/PhysRev.144.763
27. Klein Y, Hébert S et al (2006) Phys Rev B 73:052412. doi: 10.1103/PhysRevB.73.052412